

Suppression of Lamb wave excitation via aperture control of a transducer array for ultrasonic clamp-on flow metering

Massaad, J.; Neer, P. L. M. J. van; Willigen, D. M. van; Pertijs, M. A. P.; Jong, N. de; Verweij, M. D.

DOI

[10.1121/10.0001135](https://doi.org/10.1121/10.0001135)

Publication date

2020

Document Version

Final published version

Published in

Journal of the Acoustical Society of America

Citation (APA)

Massaad, J., Neer, P. L. M. J. V., Willigen, D. M. V., Pertijs, M. A. P., Jong, N. D., & Verweij, M. D. (2020). Suppression of Lamb wave excitation via aperture control of a transducer array for ultrasonic clamp-on flow metering. *Journal of the Acoustical Society of America*, 147(4), 2670-2681. <https://doi.org/10.1121/10.0001135>

Important note

To cite this publication, please use the final published version (if applicable). Please check the document version above.

Copyright

Other than for strictly personal use, it is not permitted to download, forward or distribute the text or part of it, without the consent of the author(s) and/or copyright holder(s), unless the work is under an open content license such as Creative Commons.

Takedown policy

Please contact us and provide details if you believe this document breaches copyrights. We will remove access to the work immediately and investigate your claim.

Suppression of Lamb wave excitation via aperture control of a transducer array for ultrasonic clamp-on flow metering

Jack Massaad, Paul L. M. J. van Neer, Douwe M. van Willigen, Michiel A. P. Pertijs, Nicolaas de Jong, and Martin D. Verweij

Citation: *The Journal of the Acoustical Society of America* **147**, 2670 (2020); doi: 10.1121/10.0001135

View online: <https://doi.org/10.1121/10.0001135>

View Table of Contents: <https://asa.scitation.org/toc/jas/147/4>

Published by the [Acoustical Society of America](#)

ARTICLES YOU MAY BE INTERESTED IN

[Source localization in the deep ocean using a convolutional neural network](#)

The Journal of the Acoustical Society of America **147**, EL314 (2020); <https://doi.org/10.1121/10.0001020>

[Analysis of a wooden specimen's mechanical properties through acoustic measurements in the very near field](#)

The Journal of the Acoustical Society of America **147**, EL320 (2020); <https://doi.org/10.1121/10.0001030>

[Attenuation and velocity of elastic waves in polycrystals with generally anisotropic grains: Analytic and numerical modeling](#)

The Journal of the Acoustical Society of America **147**, 2442 (2020); <https://doi.org/10.1121/10.0001087>

[Joint estimation of binaural distance and azimuth by exploiting deep neural networks](#)

The Journal of the Acoustical Society of America **147**, 2625 (2020); <https://doi.org/10.1121/10.0001155>

[A robust denoising process for spatial room impulse responses with diffuse reverberation tails](#)

The Journal of the Acoustical Society of America **147**, 2250 (2020); <https://doi.org/10.1121/10.0001070>

[Production-perception relationship of Mandarin tones as revealed by critical perceptual cues](#)

The Journal of the Acoustical Society of America **147**, EL301 (2020); <https://doi.org/10.1121/10.0000963>



CALL FOR PAPERS

JASA
THE JOURNAL OF THE
ACOUSTICAL SOCIETY OF AMERICA

Special Issue:
Lung Ultrasound

The banner features a blue background with a grid pattern and a blurred image of an ultrasound probe. A yellow box in the top right corner contains the text 'CALL FOR PAPERS'. The JASA logo is on the left, and the special issue title is in the center.

Suppression of Lamb wave excitation via aperture control of a transducer array for ultrasonic clamp-on flow metering

Jack Massaad,^{1,a)} Paul L. M. J. van Neer,^{1,b)} Douwe M. van Willigen,^{2,c)} Michiel A. P. Pertijs,^{2,d)} Nicolaas de Jong,^{1,e),f)} and Martin D. Verweij^{1,e),g)}

¹Laboratory of Medical Imaging, Department of Imaging Physics, Delft University of Technology, 2628CJ Delft, the Netherlands

²Electronic Instrumentation Laboratory, Department of Microelectronics, Delft University of Technology, 2628CD Delft, the Netherlands

ABSTRACT:

During ultrasonic clamp-on flow metering, Lamb waves propagating in the pipe wall may limit the measurement accuracy by introducing absolute errors in the flow estimates. Upon reception, these waves can interfere with the up and downstream waves refracting from the liquid, and disturb the measurement of the transit time difference that is used to obtain the flow speed. Thus, suppression of the generation of Lamb waves might directly increase the accuracy of a clamp-on flow meter. Existing techniques apply to flow meters with single element transducers. This paper considers the application of transducer arrays and presents a method to achieve a predefined amount of suppression of these spurious Lamb waves based on appropriate amplitude weightings of the transducer elements. Finite element simulations of an ultrasonic clamp-on flow measurement setting will be presented to show the effect of array aperture control on the suppression of the Lamb waves in a 1-mm-thick stainless steel pipe wall. Furthermore, a proof-of-principle experiment will be shown that demonstrates a good agreement with the simulations.

© 2020 Acoustical Society of America. <https://doi.org/10.1121/10.0001135>

(Received 11 December 2019; revised 28 February 2020; accepted 6 April 2020; published online 28 April 2020)

[Editor: Richard Daniel Costley]

Pages: 2670–2681

I. INTRODUCTION

Acoustic waves are widely used to measure flow.^{1–3} The most basic ultrasonic flow meters consist of two single-element transducers, located a certain distance apart along a pipe wall. Both transducers can be used to excite and record acoustic waves, which enable point-to-point transmission of waves that propagate upstream or downstream relative to the direction of the flow. The transit time difference between these two waves, in combination with the acoustic length of the travel paths and the wave speeds, can be used to obtain a flow speed estimate.⁴ The transducers of a flow meter can be in contact with the liquid in an in-line fashion, or be mounted on the outside of the pipe wall in a clamp-on fashion. In the latter case, the acoustic waves will make one or more bounces at the opposite pipe wall. The advantage of the clamp-on type is that they can be installed without interruption of the flow in the pipe and without affecting the mechanical strength of the pipe wall.

Unfortunately, clamp-on flow meters generate multiple wave modes, such as Lamb waves, in the pipe wall. These

are mainly caused when the acoustic waves in the fluid reflect at the pipe wall. At the receiving transducer, these modes can interfere with the longitudinal acoustic waves refracting from the liquid. This will disturb the measurement of the transit time difference between up- and down-going waves in the fluid, thus causing an absolute error in the estimation of the flow speed. Current solutions to this problem are: use of a specific incidence angle of the acoustic waves when these hit the pipe wall to minimize the excitation of the Lamb waves; liquid-dependent transmitter–receiver placement along the pipe to enable proper time-windowing of the Lamb waves; and placement of absorbing layers around the pipe wall to reduce propagation of Lamb waves.⁵ In view of Snell's law, a fixed angle of the acoustic beam in the pipe wall (e.g., defined by an angled wedge) results in a wave speed-dependent refraction angle of the beam in the liquid. This means that the travel path of the acoustic beam is liquid-dependent, and the distance between transmitter and receiver has to be modified (i.e., calibrated) accordingly for every fluid. Therefore, the dependence on the liquid prohibits a calibration-free flow meter.

Time-windowing of the longitudinal wave is not possible for all cases, since for pipe walls with a large thickness to wavelength ratio, a considerable amount of Lamb wave modes can be excited, and the probability of overlapping in time with the longitudinal wave refracting from the liquid increases. This problem is even more serious because Lamb waves are dispersive and the different Lamb wave modes have different group speeds. Moreover, the installation of

^{a)}Electronic mail: J.M.MassaadMouawad@tudelft.nl, ORCID: 0000-0002-3905-1206.

^{b)}Also at: Department of Acoustics and Sonar, TNO, 2597AK the Hague, the Netherlands, ORCID: 0000-0003-4199-4374.

^{c)}ORCID: 0000-0002-2297-4370.

^{d)}ORCID: 0000-0002-9891-4374.

^{e)}Also at: Department of Biomedical Engineering, Thorax Center, Erasmus MC, 3015 GD Rotterdam, the Netherlands.

^{f)}ORCID: 0000-0001-8902-0099.

^{g)}ORCID: 0000-0002-7441-7218.

absorbing layers around intricate pipe lines is difficult to perform in practice and sometimes not possible, especially in confined spaces. This motivates the development of an ultrasonic flow meter solution that provides Lamb suppression without compromising measurement precision, is independent of the specific liquid, and is calibration-free.

Selectivity of wave mode excitation with single-element transducers via angled wedges is described in the literature.⁶ However, by exploiting the wedge angle for Lamb wave suppression, we lose this degree of freedom for simultaneously steering the angle of the beam that will refract into the fluid. With transducer arrays and their capabilities for element-wise phase and amplitude control, considerably more control can be achieved.

There are a number of articles on suppression of transmitted Lamb waves.^{7–15} These methods are based on phase manipulation of the time domain signals for the suppression of one specific Lamb wave mode. On the other hand, methods for boosting the generation of Lamb waves in a plate via an ultrasonic array have been previously described as well.^{16–20} These are also based on phase manipulation of the time domain signals. Apart from suppression of specific Lamb wave modes in the pipe wall, during flow metering it is desired to have an acoustic beam with a very well-defined wave front and propagation direction. Although both individual goals can be achieved with manipulation of the phase, it is not possible to reach both goals simultaneously. This is because the phase appears in the exponent of the complex representation of a signal, so the addition of two phases has the effect of one overall time delay. This is appropriate for concatenated time delay effects like beam steering and beam focusing. However, phase addition does not work for effects that require two separate time delays, like simultaneously generating two beams in different directions. Because Lamb wave suppression and acoustic beam generation are effects involving two different directions, these also cannot be achieved by the addition of phases.

Separating the aperture function of a transducer array by splitting it into its amplitude and phase behavior has been used in medical imaging.^{21–23} In this article we will describe a method that uses the amplitude of the transmitting elements of an array transducer to suppress Lamb waves, while the phase of the elements is used to control the direction and shape of the acoustic beam.

II. THEORY

In this section, the relevant equations for Lamb wave propagation are described, as well as how their excitation can be controlled by means of the apodization of a transducer array.

A. Lamb waves

Lamb waves are plane elastic waves that propagate in a flat plate with traction free surfaces.^{24,25} In a cylindrical geometry (like a pipe), the mathematical treatment is analogous, using the boundary value problem for a hollow elastic cylinder.^{18,26,27} Here, we will assume that the considered pipe has a sufficiently large diameter, therefore the approximation of a flat plate can be made.²⁸ Furthermore, forward models of dispersion curves of flat plates and hollow cylinders of the same thickness (comparable to its radius) show discrepancies at frequencies that are very low to make a practical flow measurement anyway.

Lamb waves exist in the form of symmetric and anti-symmetric vibration modes, which can be further specified by their mode number. As mentioned earlier, Lamb waves are dispersive, see Fig. 1(b). Both vibration modes produce in-plane and out-of-plane particle displacement. For symmetric modes, the main motion is in-plane, while for anti-symmetric modes it is out-of-plane, as depicted in Fig. 1(a).

For an infinite plate of thickness $2h$, the Lamb modes are mathematically described by the Rayleigh–Lamb dispersion relations for symmetric modes

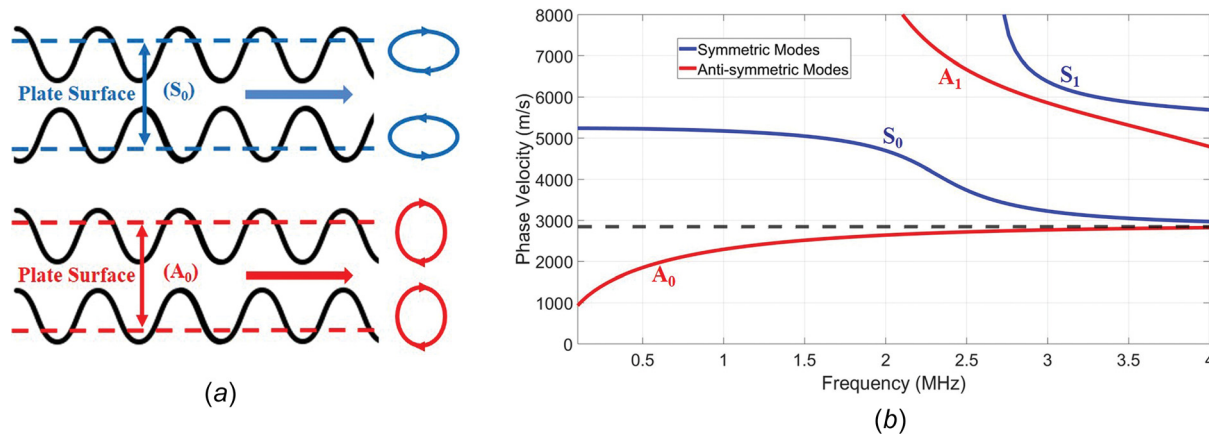


FIG. 1. (Color online) Retrograde (a) Surface motion of symmetric (S) and anti-symmetric (A) Lamb wave modes in a plate. The blue and red ellipses indicate the trajectory of particle motion at each surface of the plate. The arrows indicate the propagation direction of the wave modes. (b) Phase velocity dispersion curves of the zero and first order Lamb wave modes that can propagate along a stainless steel plate with a thickness of 1 mm ($c_L = 5800$ m/s, $c_T = 3100$ m/s). The dashed line indicates the Rayleigh wave speed c_R at a single free surface.

$$\frac{\tan(qh)}{\tan(ph)} = -\frac{4k^2pq}{(q^2 - k^2)^2}, \tag{1}$$

and for anti-symmetric modes

$$\frac{\tan(qh)}{\tan(ph)} = -\frac{(q^2 - k^2)^2}{4k^2pq}. \tag{2}$$

In Eqs. (1) and (2), p and q are defined as

$$p^2 = \left(\frac{\omega^2}{c_L^2}\right)^2 - k^2, \tag{3}$$

$$q^2 = \left(\frac{\omega^2}{c_T^2}\right)^2 - k^2.$$

In Eq. (3), ω represents the angular frequency; k represents the wavenumber; c_L and c_T the longitudinal (compressional) and transversal (shear) wave speed in the material, respectively. The solutions to the dispersion equations can be found numerically.¹⁸

The total wave field propagating in a solid slab can be expressed as the sum of symmetric and anti-symmetric mode functions for both in-plane, and out-of-plane particle motion. Considering x as the coordinate in the thickness direction, and z as the coordinate in the propagation direction, in-plane particle displacement can be mathematically expressed as

$$u(\omega, x, z) = \sum_{n=0}^{\infty} A_n(\omega) \Phi_{s,n}(\omega, x) e^{ikz} + B_n(\omega) \Phi_{a,n}(\omega, x) e^{ikz}, \tag{4}$$

where $\Phi_{s,n}(\omega, x)$ and $\Phi_{a,n}(\omega, x)$ represent the symmetric and anti-symmetric in-plane mode functions, respectively, and $A_n(\omega)$ and $B_n(\omega)$ represent the expansion coefficients of both modes.

Correspondingly, out-of-plane particle displacement can be expressed as

$$w(\omega, x, z) = \sum_{n=0}^{\infty} A_n(\omega) \Psi_{s,n}(\omega, x) e^{ikz} + B_n(\omega) \Psi_{a,n}(\omega, x) e^{ikz}, \tag{5}$$

where $\Psi_{s,n}(\omega, x)$ and $\Psi_{a,n}(\omega, x)$ represent the symmetric and anti-symmetric out-of-plane mode functions.

Mode functions $\Phi_{s,n}(\omega, x)$ and $\Phi_{a,n}(\omega, x)$ are orthogonal in x . This property allows us to compute an expression for the expansion coefficients $A_n(\omega)$ and $B_n(\omega)$, at some location $z = z_0$

$$A_n(\omega) = \frac{\int_a^b u(\omega, x, z_0) \Phi_{s,n}^*(\omega, x) e^{-ikz_0} dx}{\int_a^b \Phi_{s,n}(\omega, x) \Phi_{s,n}^*(\omega, x) dx}, \tag{6}$$

$$B_n(\omega) = \frac{\int_a^b u(\omega, x, z_0) \Phi_{a,n}^*(\omega, x) e^{-ikz_0} dx}{\int_a^b \Phi_{a,n}(\omega, x) \Phi_{a,n}^*(\omega, x) dx}. \tag{7}$$

The limits of the integrals in Eqs. (6) and (7) comprise the thickness of the solid slab being examined, and * indicates the complex conjugate. For each frequency, the expansion coefficients indicate the importance of the contribution of a particular mode to the total field distribution. The location z_0 should be outside the area where the modes are generated, i.e., outside the transducer range.

Frequency dependence of the amplitudes of the zero-order Lamb wave modes for a 5-mm-thick stainless steel plate is shown in Fig. 2. Even though an appropriate excitation frequency can help with the suppression of Lamb waves by a factor of 2, it is often not enough to achieve the needed accuracy for clamp-on flow metering.

B. Beam transmission with transducer arrays

Ultrasonic arrays have been designed and used for different purposes including medical imaging and Non Destructive Evaluation (NDE).²⁹ The far field directivity pattern of the acoustic beam produced by a transducer array consisting of rectangular elements radiating into a half-space can be described by the directivity function²³

$$D(\theta) = dsinc\left(-\frac{d}{\lambda} \sin \theta\right) \sum_{n=-(N-1/2)}^{N-1/2} F_n e^{in(\Delta\phi_n + kd \sin \theta)}, \tag{8}$$

in which the amplitude F_n and phase $\Delta\phi_n$ of each element are parts of the complex apodization or aperture function $F_n \exp(i\Delta\phi_n)$ in the Fourier domain. Moreover, d is the pitch of the array; θ is the observation angle relative to the normal on the transducer surface, and N is the total number of elements of the array. In a clamp-on flow measurement setting, λ is the wavelength in the liquid.

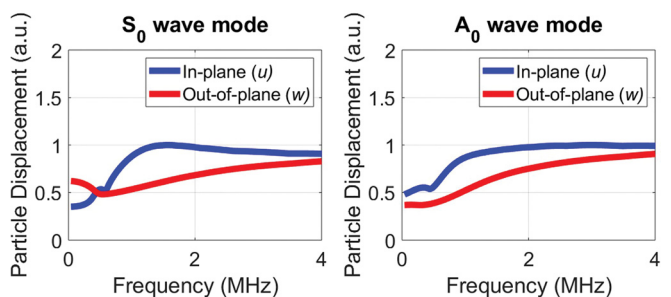


FIG. 2. (Color online) Amplitudes of the particle displacement of the zero-order Lamb waves in a 5-mm-thick stainless steel plate, loaded by water on one side, and by vacuum on the other side. A transducer array, placed on the vacuum-loaded surface of the plate, was used to excite an acoustic beam that impinged the steel–water interface with an angle of 45°. The displacements $u(\omega, x, z_0)$ and $w(\omega, x, z_0)$ were computed across the thickness of the pipe wall ($-h \leq x \leq h$), at a propagation distance (z_0) located at the edge of the transducer array.

Considering Eq. (8) in an ultrasonic clamp-on flow measurement setting, the transducer array is virtually placed in the pipe wall–liquid interface. Furthermore, the effect of the pipe wall on Eq. (8) is directly observed in Fig. 3, by the amount of energy located beyond the critical angles of the Lamb wave modes. These angles depend on Snell’s law through the sound speed of each mode at a particular frequency (1 MHz in case of Fig. 3) and the sound speed of the liquid.

During flow metering, significant Lamb wave modes are excited each time the acoustic beam impinges from the liquid onto the pipe wall. Such wave modes are excited even more efficiently when the incidence angle is close to their critical angle³⁰ (Fig. 3). Therefore, it may be necessary to suppress the amount of energy leaking into Lamb wave excitation at each beam reflection. Proper phase control of the transmitting array may result in steering the incidence angle as to avoid excitation of Lamb waves.²⁰ In contrast to previous work, in this research the phase shifts $\Delta\phi_n$ are reserved to steer and shape the beam, and the amplitude factors F_n are manipulated to suppress, the generation of undesired Lamb waves at each reflection of the acoustic beam.

III. ALGORITHM

The beam spot width W of an acoustic beam that hits the pipe wall with an incident angle θ relative to the normal of the pipe wall, can be computed as

$$W = \frac{2L \tan(\alpha/2)}{\cos \theta} \tag{9}$$

Here, α is the opening angle of the beam at the -3 dB power level, and L is the distance travelled by the acoustic beam, i.e., the total length of the beam path from transmitter to receiver.

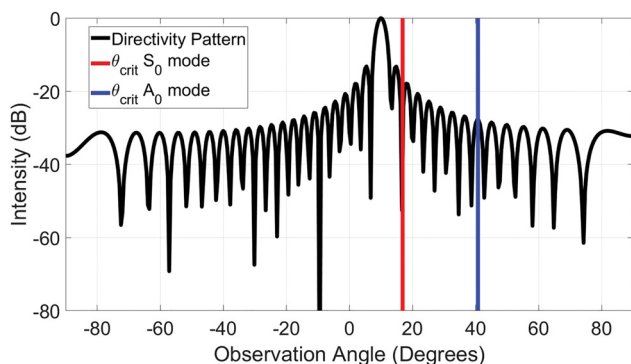


FIG. 3. (Color online) Directivity pattern (black curve) of a $\Psi = 10^\circ$ -steered acoustic beam in water ($c_m = 1500$ m/s) produced by a 37-element transducer array with a pitch of 0.72 mm excited at 1 MHz. To compute it, Eq. 8 was implemented, where $F_n = 1$, and $\Delta\phi_n = nkd \sin(\Psi)/c_m$, with k being the wavenumber of the acoustic beam in water at 1 MHz. The vertical red and blue lines indicate the critical angles beyond which only the zero-order Lamb wave modes propagate when such a beam impinges on a 1-mm-thick stainless-steel pipe wall. Due to the presence of side lobes, some energy from the beam may leak into these Lamb modes.

In clamp-on flow metering, the best accuracy is achieved when a maximum signal-to-noise ratio (SNR) is reached. This occurs when the entire aperture of the array is insonified by the entire in-coming beam. Therefore, it is desired to have an array aperture of N array elements that allows one to generate a narrow acoustic beam on the transmission side and also to record this beam on all N elements on the receiving side. In receive, this will average out the noise by a factor of \sqrt{N} compared to a single element.

However, such beams require small opening angles, and therefore demand a considerable number of elements. Cost and complexity of application-specific integrated circuits (ASICs) are proportional to the number of elements needed to drive a transducer array, and may become prohibitive for the number of elements that are needed to produce theoretically ideal beams. In practice, only a limited number of elements will be available, which will have an impact on the beam. Therefore, we have to find a way to reduce the number of elements while retaining a good signal-to-noise ratio and a sufficient suppression of Lamb waves.

A flowchart of our algorithm to achieve this is shown in Fig. 4, and will be described in detail below

A. Step 1: Define known parameters for beam and transducer

First, the known parameters for the beam and the transducer are set. These are the length L of the travel path of the beam, the level s of the first side lobe relative to the level of the main beam, and the pitch p of the array. These parameters are application dependent. Moreover, we will set an initial number of e array elements. An as example we will design a transducer array with a center frequency of 1 MHz. Moreover, we will consider a pipe inner diameter of 40 mm, and a beam propagating in water under an angle of $\theta = 10^\circ$ with the normal of the pipe wall and making six bounces (“v”-shapes) within the pipe. For this geometry, a travel path length $L = 488$ mm can be determined.

Moreover, we will assume, as an external demand, that a suppression $s = 35$ dB of the spurious Lamb waves is needed. As a worst case scenario, we assume that all side lobes of the acoustic beam are converted into spurious Lamb modes, and that side lobe and Lamb mode amplitude are equivalent.

For a frequency band up to 2 MHz, a pitch $p = 0.72$ mm was considered to properly sample all possible propagating Lamb wave modes in stainless steel pipes with wall thicknesses between 1 and 5 mm.

A relatively large number of array elements e is recommended to produce a narrow beam in reception and to ensure that all of its energy gets recorded. As an example, we explain the algorithm by showing the results with $e = 152$ initial array elements.

B. Step 2: Compute desired beam

To achieve the desired suppression level, the element amplitudes F_n in Eq. (8) were set to form a Blackman

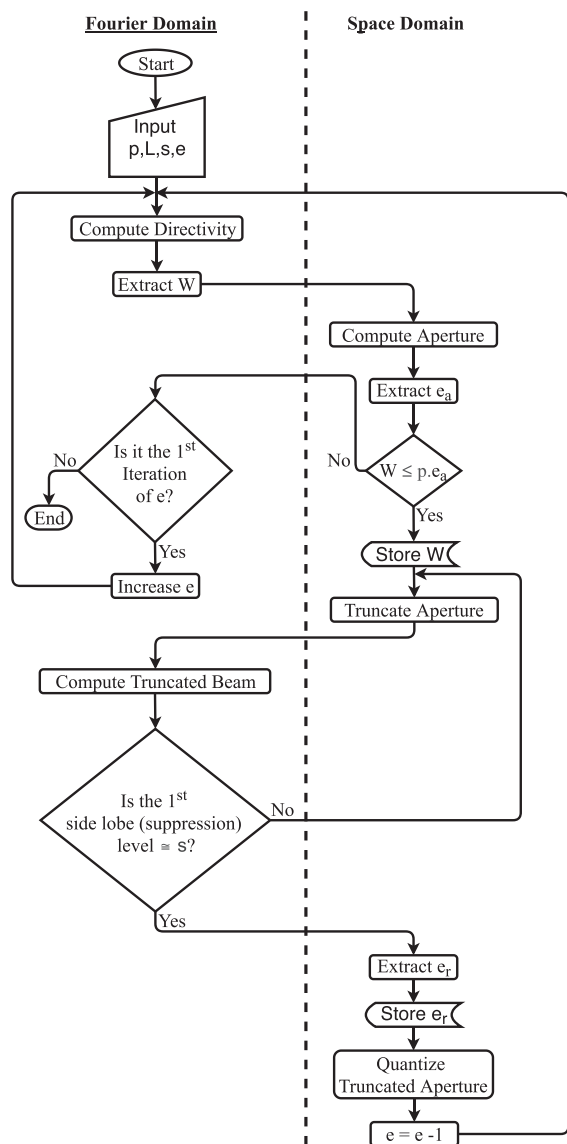


FIG. 4. Flowchart of the proposed algorithm to obtain a transducer array aperture giving a good signal-to-noise ratio and sufficient suppression of Lamb waves. The ideal transmit beam yields a receive beam spot width that is equal to the recording array aperture.

window. Figure 5(a) shows that the first side lobe is conveniently below the required 35 dB level. Furthermore, at the -3 dB level, the beam has an opening angle $\alpha = 3^\circ$ in water, which according to Eq. (9), produces a beam spot width $W = 25.1$ mm upon reception.

C. Step 3: Compute desired aperture

The aperture to produce the beam shown in Fig. 5(a) is computed via the inverse fast Fourier transform (IFFT) of Eq. (8). The obtained aperture in Fig. 5(b) suggests that $e_a = 50$ active elements are sufficient to produce such a beam. The corresponding effective aperture of 36 mm ensures that the whole beam width gets recorded upon reception. Otherwise, the algorithm would ask for a higher initial number of array elements e to produce a narrower beam.

D. Step 4: Truncate aperture and extract residual active elements

The challenge is to reduce the number of elements e below the obtained number of active elements e_a . Aperture truncation in the space domain is performed by multiplying the function in Fig. 5(b) with a rectangular window. This has the physical meaning of reducing the total number of elements of the array [red curve in Fig. 5(c)], at the cost of increasing the side lobe levels compared to the initial beam. In this case, truncation is performed until the amplitude of the first side lobe reaches 35 dB [red curve in Fig. 5(d)]. This resulted in $e_r = 37$ residual active elements, which cover an aperture of 26.6 mm.

E. Step 5: Quantize the truncated aperture

In practical electronic transmit circuits, the amplitudes F_n of the elements will be quantized, and the aperture will have a step-like shape. In the current case we have applied a 4 bit-quantization of the aperture [black curve in Fig. 5(c)]. This further modifies the shape of the resultant beam.

F. Step 6: Compute practical beam

By again invoking Eq. (8), the beam resulting from the truncated and quantized aperture can be obtained. At this stage it is possible to see whether the quantization still leads to an acceptable performance. For the described 4-bit case, the beam has a very similar width as the non-quantized one and keeps the side lobe levels below 35 dB [black curve in Fig. 5(d)]. Higher quantization levels would produce a smoother aperture, but the complexity of the electronics would increase proportionally. Last, the -3 dB opening angle α can be extracted and the spot width W of the quantized beam can be computed. In this case, the beam has an opening angle $\alpha = 3.1^\circ$ and produces a beam spot width $W = 26.1$ mm upon reception, which is close to the 26.6 mm size of the array aperture.

The algorithm will loop steps 2–6 with a smaller initial number of array elements e . This happens until the beam spot width becomes larger than the residual active array aperture. Figure 6 shows the beam spot size upon reception, as a function of the aperture size. From this figure it is possible to graphically find the optimal number of array elements for the ultrasonic clamp-on flow metering application: the one whose aperture has the same (or very similar) length as the produced beam spot width upon reception.

IV. SIMULATION STUDY

In this section, two dimensional (2D) simulations are presented for a water-filled stainless steel pipe with 40 mm inner diameter and 1 mm wall thickness, in combination with a transducer array with a pitch of 0.72 mm clamped outside the pipe wall. Furthermore, two different center frequencies will be considered in two separate scenarios: 1 and 1.5 MHz. The first one will be the center frequency of a sensor under development, and the second one is the center frequency used in experimental studies presented in Sec. VA.

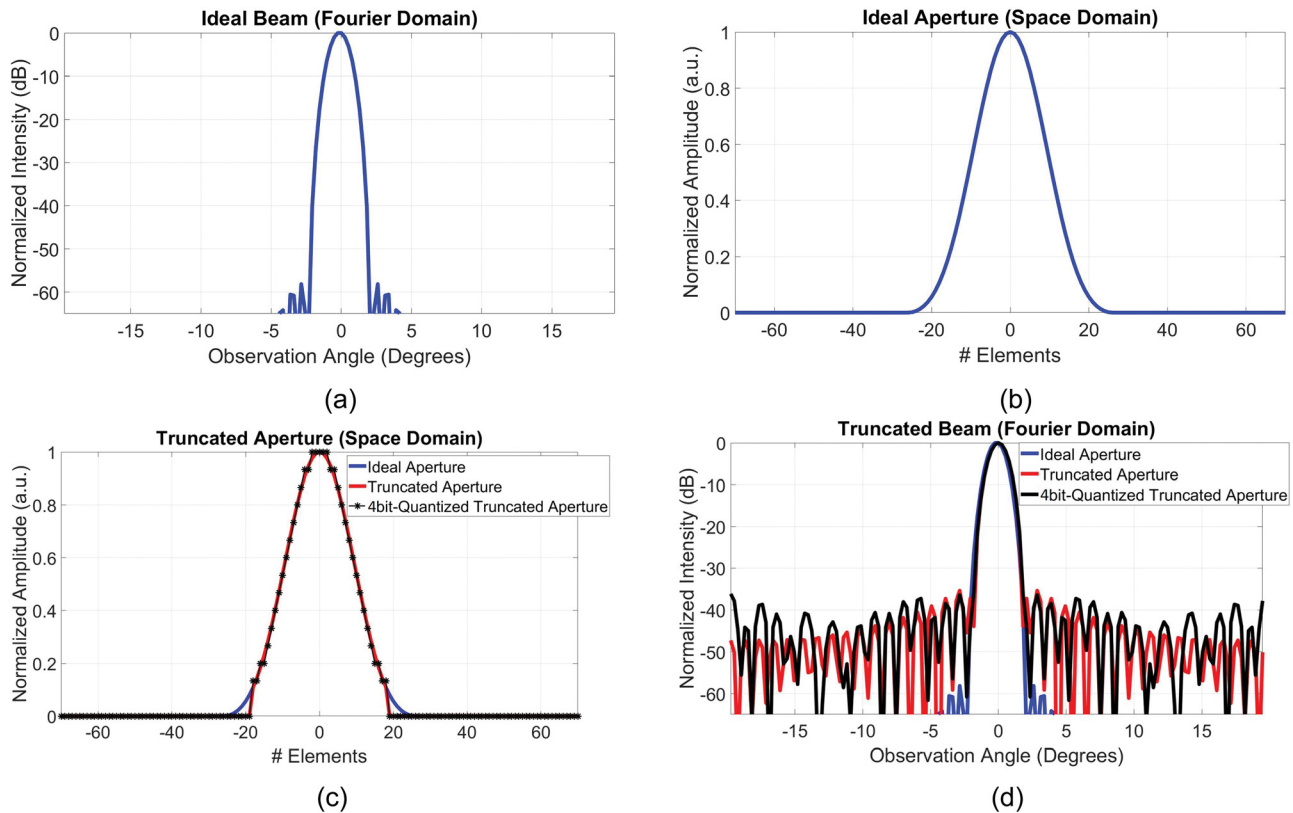


FIG. 5. (Color online) Beams and apertures involved in the design of a 1 MHz-transducer array with a 0.72 mm pitch for ultrasonic clamp-on flow measurements, capable of suppressing Lamb waves of a 1-mm-thick stainless steel wall by 35 dB during transmission. (a) Ideally desired beam: small opening angle and low side lobe levels. (b) Aperture function that shows an unpractical number of active elements needed to produce the ideal beam. (c) Truncated aperture function obtained with a rectangular window (red curve). After truncation, the aperture region with non-zero amplitudes is quantized (black curve). (d) Effect of truncation: rise of the side lobes relative to the ideal beam (red curve), and of quantization: small variation in side lobe levels (black curve).

A. Simulation settings

At 1 MHz, the fastest Lamb wave mode that can propagate in a 1-mm-thick stainless steel pipe wall is the zero-order symmetric (S_0) mode [$c_{S_0} = 5173$ m/s, see Fig. 1(b)]. It was found in Sec. III that 37 elements are enough to produce a 35 dB suppression of this mode. In this case, a beam steered at 45° through the pipe wall would refract into water

at 10° with an opening angle of 3.1° , which is below the critical angle for the S_0 mode, being 16.9° .

On the other hand, to suppress the S_0 wave mode at 1.5 MHz, the implementation of the algorithm proposed in Sec. III would report an optimal $e_r = 25$ residual active elements (aperture of 18 mm) with a beam spot width of $W = 18.64$ mm upon reception. Considering the dispersion curves of Fig. 1(b), and the same 10° angle of refraction of the acoustic beam into the water, it is expected to suppress the S_0 wave mode, and also to have some leakage towards the excitation of the A_1 wave mode since this last one has a faster sound speed, relative to the S_0 wave mode, that is not accounted by the beam direction.

Two-dimensional finite element modeling (FEM) was used to simulate the effect of controlling the amplitudes of the elements of a transducer array for the suppression of Lamb waves. The software package PZFlex (Onscale, Redwood City, CA) was used. A 2D longitudinal cross section of a water-filled pipe was defined [Fig. 7(a)], including an array consisting of lead-zirconate-titanate (PZT) elements made of HK1HD (TRS Technologies, Inc., State College, PA).

For each scenario (i.e., center frequency), two simulations were carried out. In both, the driving function on the PZT elements consisted of a two-cycle sine wave, and the acoustic beam was steered 45° by means of phase shifting.

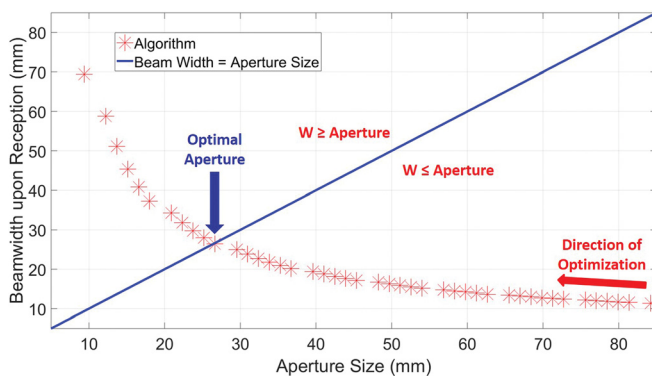


FIG. 6. (Color online) Beam spot width upon reception as a function of aperture size, as computed by the algorithm, for a 1 MHz transducer array with a 0.72 mm pitch and 35 dB suppression of Lamb waves. The optimal aperture size of 26.6 mm corresponds to 37 array elements.

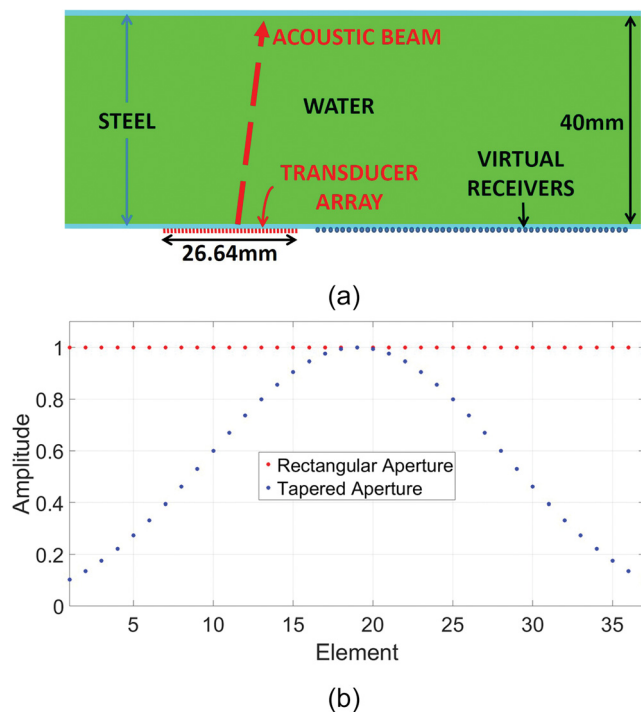


FIG. 7. (Color online) (a) Cross-section of the pipe used in 2D FEM simulations of a 37-element transducer array with a center frequency of 1 MHz. The acoustic beam was steered 45° through the 1-mm-thick pipe wall, traveling to the right. Stress perpendicular to the steel surface was recorded by the virtual receivers to identify propagating waves in post-processing. (b) Amplitude function (F_n) applied to the driving signals of the elements.

For the first simulation, a uniform amplitude function was applied to the driving signals of the elements. For the second simulation, a tapered amplitude function obtained by the previously described algorithm was applied [Fig. 7(b)]. Virtual receivers were placed along the steel–air interface to

record the total perpendicular stress component from all waves in the pipe wall, including the longitudinal wave refracting from the liquid. These waves were subsequently identified in the Fourier domain. The simulations were run until the beams had bounced six times (v-shapes) within the pipe.

B. Results for 1 MHz

For the applied uniform and tapered amplitudes, the stress component perpendicular to the steel surface is shown in Figs. 8(a) and 8(b). In Fig. 8(a) the excitation of Lamb waves at each bounce of the beam is visible, and in Fig. 8(b) it is shown that these waves are highly suppressed. To demonstrate the working of the algorithm, the geometry in Fig. 7(a) was chosen such that the longitudinal wave and the Lamb waves are independently visible in the time domain.

The magnitude of the 2D fast Fourier transform (FFT) of the time signals in Fig. 8 was computed to quantitatively get the amount of Lamb wave suppression achieved in each case. Figure 9 shows the independently normalized magnitudes with a dynamic range of 35 dB. It can be noticed that, after the implementation of a tapered amplitude function [Fig. 9(b)], the S_0 Lamb wave mode was suppressed below 35 dB, as desired.

The striped nature of the information in Fig. 9 is a result of applying an FFT to the entire time-space domain of Fig. 8 rather than to individual echoes. Furthermore, the side lobes located around 0.25 and 1.7 MHz are the result of space-time windowing effects of the signal.

C. Results for 1.5 MHz

The time signals in Fig. 10 show the effect of a suppression of the Lamb wave modes when a tapered aperture of the transducer array is implemented. Moreover, the 2D FFTs shown in Fig. 11 quantitatively indicate a suppression

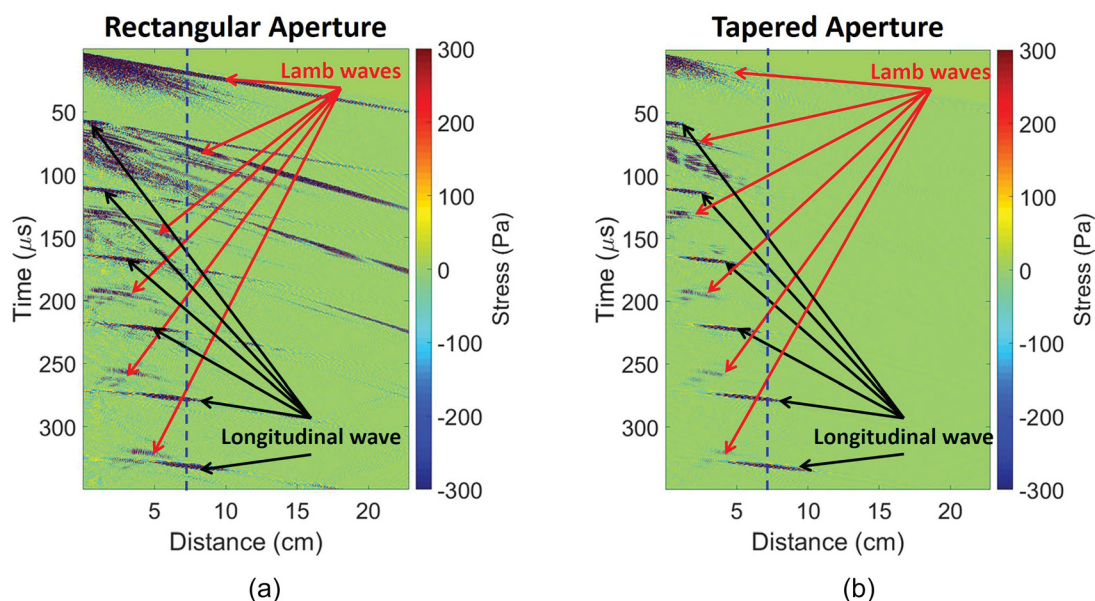


FIG. 8. (Color online) Stress (perpendicular component) recorded along the steel–air interface for the two considered simulations. (a) Rectangular aperture function (b) Tapered aperture function. The longitudinal wave refracting from water bounced six times within the pipe wall. The blue dashed lines mark the time signal located 7.7 cm away from the source.

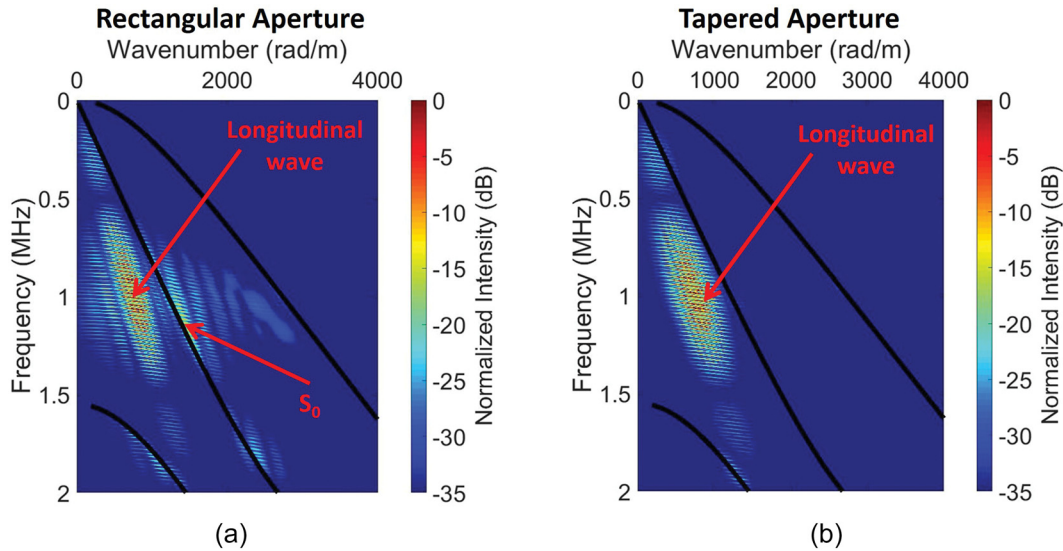


FIG. 9. (Color online) Normalized 2D FFT of the recorded space-time signals in Fig. 8 for the two considered simulations (a) Rectangular aperture function. (b) Tapered aperture function. The black lines represent the theoretical dispersion curves of the Lamb waves that propagate within the steel.

of the amplitude of the problematic S_0 Lamb wave mode by 35 dB relative to the longitudinal wave refracting from the liquid, as designed and expected from the algorithm described in this article.

As expected, it is also possible to see in Fig. 11(b) that besides suppression of the S_0 wave mode, some energy leaks towards the A_1 wave mode at around 2 MHz due to the faster mode speed (i.e., smaller critical angle). When this situation becomes an issue, some options can be considered in practice: steer the acoustic beam according to the fastest expected Lamb wave mode around the center frequency of the array, and/or use a more narrow-banded pulse.

In view of the previously described points, the signals leading to Figs. 9(b) and 11(b) will make a more accurate

estimate of flow relative to those of Figs. 9(a) and 11(a), since the disturbing Lamb wave mode (in particular the one closest to the longitudinal wave carrying information from the water) has been suppressed below the required level. If necessary, other types of methods (e.g., filtering, time windowing) can be applied afterwards to suppress less problematic spurious Lamb waves.

V. EXPERIMENTAL VALIDATION OF THE METHOD

A. Measurement description

For a proof of principle, the experimental setup of Fig. 12 was built. It consisted of two 1-mm-thick parallel stainless-steel plates separated by a 40 mm column of water.

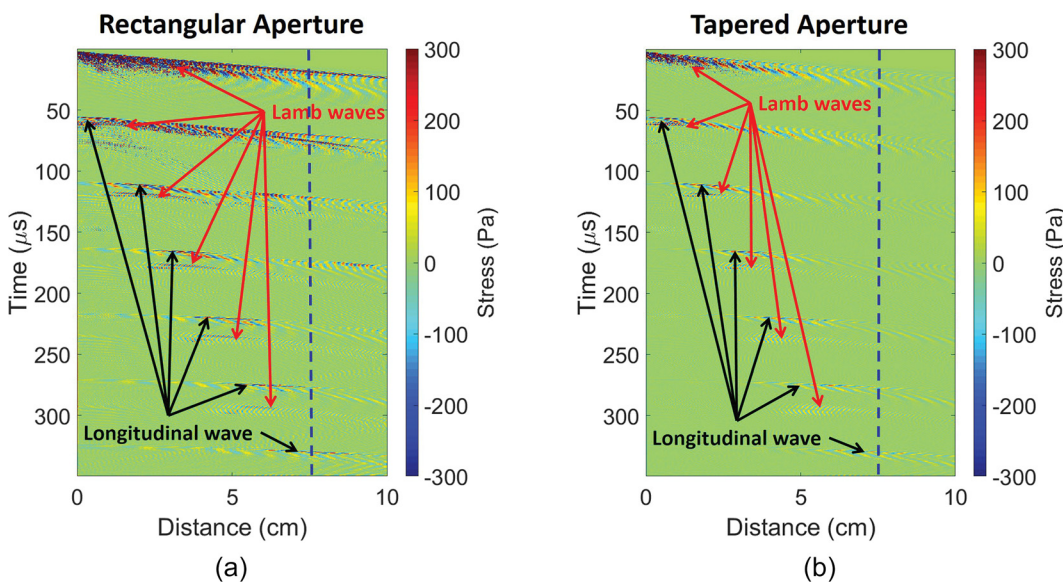


FIG. 10. (Color online) Stress (perpendicular component) recorded along the steel–air interface for simulations considering a 25-element transducer array with a center frequency of 1.5 MHz. (a) Rectangular aperture function (b) Tapered aperture function. The longitudinal wave refracting from water bounced six times within the pipe wall. The blue dashed lines mark the time signal located 7.7 cm away from the source.

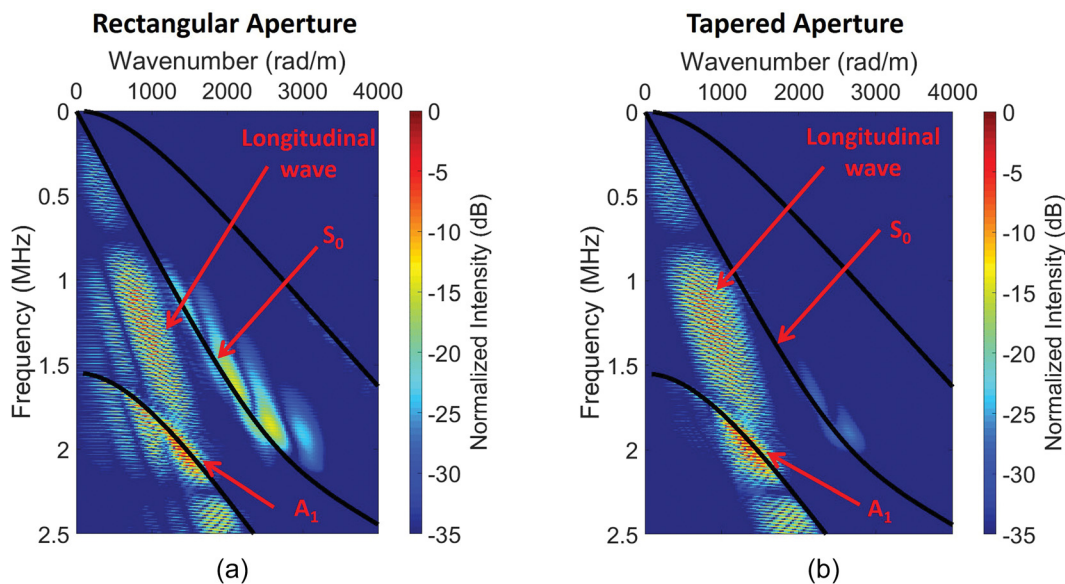


FIG. 11. (Color online) Normalized 2D FFT of the recorded space-time signals in Fig. 10 for the simulations considering a 25-element transducer array with a center frequency of 1.5 MHz. (a) Rectangular aperture function. (b) Tapered aperture function. The black lines represent the theoretical dispersion curves of the Lamb waves that propagate within the steel.

Two ATL P4-1 phased array probes (Philips, Bothell, WA) were horizontally aligned and placed on top of one of the plates. These probes consist of 96 single elements with a pitch of 295 μm and a -20 dB frequency bandwidth from 1 to 4 MHz. A Verasonics Vantage 256 (Verasonics Inc., Kirkland, WA) system was used to drive the probes and record the data.

In transmission, a 16-cycle sine wave with a center frequency of 1.5 MHz was used as a driving signal of one of the probes. Moreover, time delays were applied to its individual elements to excite a longitudinal wave in the steel plate that impinges the steel-water interface under a 45° angle. In reception, the second probe was horizontally placed 7.7 cm away from the first one (center to center distance), where according to the simulation results in Figs.

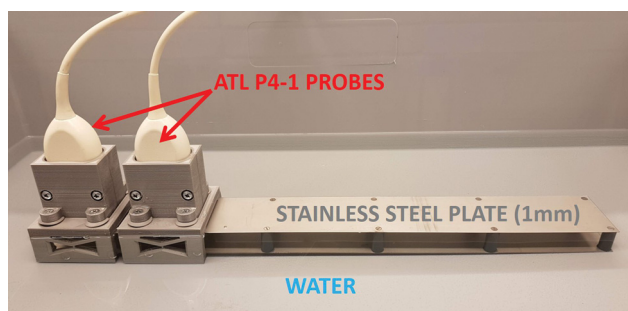


FIG. 12. (Color online) Experimental setup. Two ATL P4-1 phased array probes on top of one of the two 1-mm-thick stainless steel plates. The center of the probes were separated by 7.7 cm. The distance between both plates was 40 mm and filled with water. The upper side of the top plate was still loaded by air. Probe holders are made of a material with a similar acoustic impedance as that of water to avoid reflection effects on the recorded data.

8 and 10, it is expected to receive the fifth bounce of the longitudinal wave.

Two experiments were performed. First, a rectangular amplitude weighting function was applied along the elements of the array. Second, a tapered aperture was applied. This aperture was computed using the algorithm previously described.

B. Results and discussions

Figure 13 shows the recorded time signals for each case with all elements of the receiving probe. Five bounces of the beam can be noticed. Due to the bounded spatial region where these signals were recorded (6.3–9.1 cm away from the center of the transmitting probe), it is not as straightforward to identify different propagating wave modes in this domain as it is in Figs. 8 and 10.

Several transformations, like the Radon transform, can be used to identify the recorded wave modes.³¹ In our case, the magnitude of a 2D FFT of the measured signals in Fig. 13 was computed for identifying the propagating wave modes. Figure 14 shows the independently normalized magnitudes for each aperture with a dynamic range of 35 dB, where the longitudinal wave as well as the S_0 Lamb wave mode can be observed. With a controlled aperture, a suppression of 20 dB for the S_0 wave mode was achieved. The stripe patterns are due to the implementation of the FFT for the full space-time domain.

The space-limited information of our 2.83 cm probe aperture gives a less clear suppression effect in Fig. 14(b) relative to Fig. 11(b). Therefore, a fairer one-to-one comparison was made. The 2D FFTs of the simulated data were computed using the same spatial range as in the experiments. The difference between both aperture schemes was

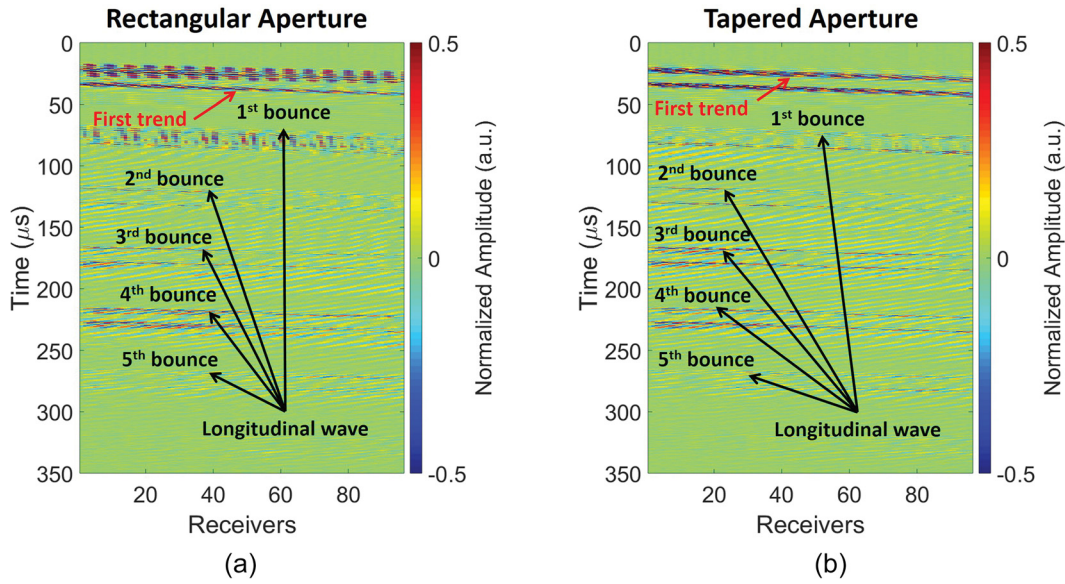


FIG. 13. (Color online) Signals recorded with all 96 elements of the receiving probe in the experimental setup. (a) Rectangular aperture function. (b) Tapered aperture function. It becomes challenging to identify the fifth bounce of the longitudinal wave in this domain.

computed and compared to that of the experimental data (see Fig. 15). It is observed that the level of suppression of the problematic S_0 Lamb wave mode, within the spatial range of the receiving transducer, is the same for the simulated and measured data, i.e., around 20 dB. Moreover, during suppression, no reduction of the energy of the longitudinal wave took place, as can also be seen in Fig. 14(b).

VI. CONCLUSIONS

In this paper, a method has been described to steer an acoustic beam through a pipe wall while suppressing, in

transmission, the excitation of spurious Lamb waves. In this way, absolute errors caused by these waves during clamp-on flow metering can be reduced. An algorithm to estimate the transducer array aperture (i.e., the number of elements and their amplitudes) required to achieve a desired performance has been described.

Due to its particular application for clamp-on flow metering, the method is based on amplitude manipulations of the aperture function of a transducer array, while phase shifts are used to control the shape of the propagating acoustic beam. Simulations and experimental results of an ultrasonic clamp-on flow measurement setting using 1-mm-thick

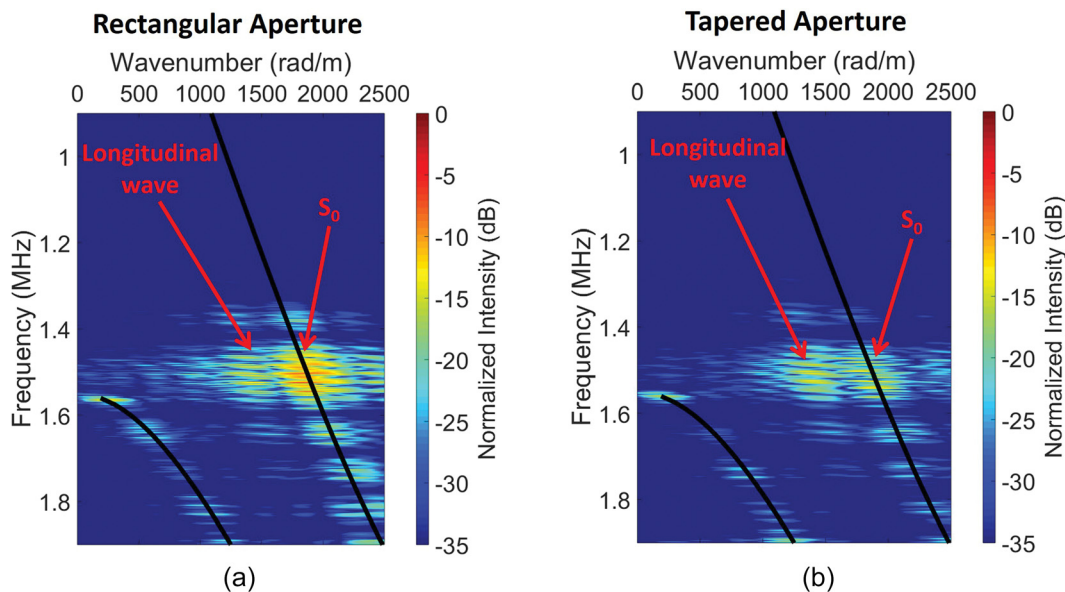


FIG. 14. (Color online) Normalized 2D FFT of the measured space-time signals in Fig. 13. (a) Rectangular aperture function. (b) Tapered aperture function. The black lines represent the theoretical dispersion curves of the Lamb waves that propagate in the steel plate.

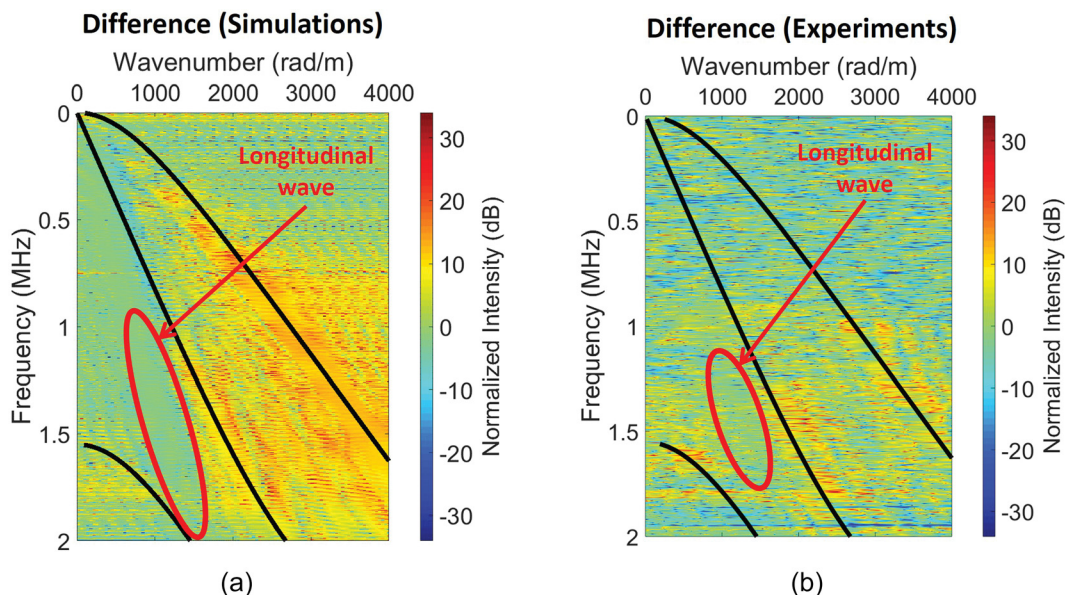


FIG. 15. (Color online) Difference between 2D FFTs of space-time signals for a rectangular and a tapered aperture. The spatial domain is located at 6.3–9.1 cm away from the center of the source. (a) Simulations. (b) Experiments. The black lines represent the theoretical dispersion curves.

stainless steel plates have been performed as proof and show a good agreement.

ACKNOWLEDGMENTS

This work is part of the research programme FLOW+, which is financed by the Dutch Technology Foundation STW (project 15031) and industrial partners Bronkhorst and KROHNE.

¹J. C. Wendoloski, "On the theory of acoustic flow measurement," *J. Acoust. Soc. Am.* **110**(2), 724–737 (2001).
²W.-S. Cheung, H.-S. Kwon, K.-A. Park, and J.-S. Paik, "Acoustic flowmeter for the measurement of the mean flow velocity in pipes," *J. Acoust. Soc. Am.* **110**(5), 2308–2314 (2001).
³R. C. Baker, *Flow Measurement Handbook: Industrial Designs, Operating Principles, Performance, and Applications* (Cambridge University Press, London, 2005).
⁴D. Kurniadi and A. Trisnobudi, "A multi-path ultrasonic transit time flow meter using a tomography method for gas flow velocity profile measurement," *Part. Part. Syst. Charact.* **23**(3-4), 330–338 (2006).
⁵M. Sanderson and H. Yeung, "Guidelines for the use of ultrasonic non-invasive metering techniques," *Flow Meas. Instrum.* **13**(4), 125–142 (2002).
⁶K. Xu, D. Ta, B. Hu, P. Laugier, and W. Wang, "Wideband dispersion reversal of Lamb waves," *IEEE Trans. Ultrason., Ferroelectr., Freq. Control* **61**(6), 997–1005 (2014).
⁷C. Prada and M. Fink, "Separation of interfering acoustic scattered signals using the invariants of the time-reversal operator. Application to Lamb waves characterization," *J. Acoust. Soc. Am.* **104**(2), 801–807 (1998).
⁸K. G. Sabra, A. Srivastava, F. Lanza di Scalea, I. Bartoli, P. Rizzo, and S. Conti, "Structural health monitoring by extraction of coherent guided waves from diffuse fields," *J. Acoust. Soc. Am.* **123**(1), EL8–EL13 (2008).
⁹K. Xu, D. Ta, P. Moilanen, and W. Wang, "Mode separation of Lamb waves based on dispersion compensation method," *J. Acoust. Soc. Am.* **131**(4), 2714–2722 (2012).
¹⁰G. Dib, O. Karpenko, M. Haq, L. Udpa, and S. Udpa, "Advanced signal processing algorithms in structural integrity monitoring," *Procedia Eng.* **86**, 427–439 (2014).

¹¹J.-L. Le Calvez and T. M. Brill, "A method to separate flexural and extensional signals from mixed-mode ultrasonic signals," in *Ultrasonics Symposium (IUS), 2016 IEEE International* (IEEE, New York, 2016), pp. 1–4.
¹²L. Bai, K. Xu, N. Bochud, D. Ta, B. Hu, P. Laugier, and J.-G. Minonzio, "Multichannel wideband mode-selective excitation of ultrasonic guided waves in long cortical bone," in *2016 IEEE International Ultrasonics Symposium (IUS)* (IEEE, New York, 2016), pp. 1–4.
¹³H. Li, X. Liu, and L. Bo, "A novel method to analysis strong dispersive overlapping Lamb-wave signatures," *J. Vibroeng.* **19**(1), 641–656 (2017).
¹⁴F. Gao, L. Zeng, J. Lin, and Z. Luo, "Mode separation in frequency–wavenumber domain through compressed sensing of far-field Lamb waves," *Meas. Sci. Technol.* **28**(7), 075004 (2017).
¹⁵V. Serey, N. Quaegebeur, P. Micheau, P. Masson, M. Castaings, and M. Renier, "Selective generation of ultrasonic guided waves in a bi-dimensional waveguide," *Struct. Health Monit.* **18**(4), 1324–1336 (2019).
¹⁶W. Zhu and J. L. Rose, "Lamb wave generation and reception with time-delay periodic linear arrays: A BEM simulation and experimental study," *IEEE Trans. Ultrason. Ferroelectr. Freq. Control* **46**(3), 654–664 (1999).
¹⁷J. Li and J. L. Rose, "Implementing guided wave mode control by use of a phased transducer array," *IEEE Trans. Ultrason. Ferroelectr. Freq. Control* **48**(3), 761–768 (2001).
¹⁸J. L. Rose, *Ultrasonic Guided Waves in Solid Media* (Cambridge University Press, London, 2014).
¹⁹K.-C. T. Nguyen, L. H. Le, T. N. Tran, M. D. Sacchi, and E. H. Lou, "Excitation of ultrasonic Lamb waves using a phased array system with two array probes: Phantom and *in vitro* bone studies," *Ultrasonics* **54**(5), 1178–1185 (2014).
²⁰C. Adams, S. Harput, D. Cowell, T. M. Carpenter, D. M. Charutz, and S. Freear, "An adaptive array excitation scheme for the unidirectional enhancement of guided waves," *IEEE Trans. Ultrason. Ferroelectr. Freq. Control* **64**(2), 441–451 (2017).
²¹D. Guyomar and J. Powers, "A Fourier approach to diffraction of pulsed ultrasonic waves in lossless media," *J. Acoust. Soc. Am.* **82**(1), 354–359 (1987).
²²R. J. Zemp, J. Tavakkoli, and R. S. Cobbold, "Modeling of nonlinear ultrasound propagation in tissue from array transducers," *J. Acoust. Soc. Am.* **113**(1), 139–152 (2003).
²³R. S. Cobbold, *Foundations of Biomedical Ultrasound* (Oxford University Press, UK, 2006).
²⁴V. Pagneux, "Revisiting the edge resonance for Lamb waves in a semi-infinite plate," *J. Acoust. Soc. Am.* **120**(2), 649–656 (2006).

- ²⁵J. D. N. Cheeke, *Fundamentals and Applications of Ultrasonic Waves* (CRC Press, Boca Raton, FL, 2016).
- ²⁶I. A. Viktorov, *Rayleigh and Lamb Waves: Physical Theory and Applications* (Plenum, New York, 1967).
- ²⁷R. Bunney, R. Goodman, and S. Marshall, "Rayleigh and Lamb waves on cylinders," *J. Acoust. Soc. Am.* **46**(5B), 1223–1233 (1969).
- ²⁸A. Velichko and P. D. Wilcox, "Excitation and scattering of guided waves: Relationships between solutions for plates and pipes," *J. Acoust. Soc. Am.* **125**(6), 3623–3631 (2009).
- ²⁹R. M. Levine and J. E. Michaels, "Model-based imaging of damage with Lamb waves via sparse reconstruction," *J. Acoust. Soc. Am.* **133**(3), 1525–1534 (2013).
- ³⁰V. Dayal and V. K. Kinra, "Leaky Lamb waves in an anisotropic plate. I: An exact solution and experiments," *J. Acoust. Soc. Am.* **85**(6), 2268–2276 (1989).
- ³¹K. Xu, D. Ta, D. Cassereau, B. Hu, W. Wang, P. Laugier, and J.-G. Minonzio, "Multichannel processing for dispersion curves extraction of ultrasonic axial-transmission signals: Comparisons and case studies," *J. Acoust. Soc. Am.* **140**(3), 1758–1770 (2016).